Catalysis Today 180 (2012) 167–173

Contents lists available at ScienceDirect

Catalysis Today

journal homepage: www.elsevier.com/locate/cattod

Synthesis of ceria-praseodimia nanotubes with high catalytic activity for CO oxidation

Leandro González Rovira, Juan José Delgado, Khadija ElAmrani, Eloy del Rio, Xiaowei Chen, José Juan Calvino, Francisco Javier Botana*

Department of Materials Science and Metallurgical Engineering and Inorganic Chemistry, University of Cádiz, República Saharaui s/n, 11510 Puerto Real, Cádiz, Spain

ARTICLE INFO

Article history:
Received 2 February 2011
Received in revised form 29 April 2011
Accepted 12 May 2011
Available online 30 July 2011

Keywords:
Cerium
Praseodymium
Template-based electrodeposition
Nanotube
CO oxidation

ABSTRACT

Ceria-praseodimia nanotubes ($Ce_{0.8}Pr_{0.2}O_{2-\delta}$–NT) have been synthesized for the first time employing a template-based electrodeposition method inside the pores of anodic aluminum oxide (AAO) membranes. Various electron microscopy techniques such as Field Emission Gun Scanning Electron Microscopy (FEG-SEM), Scanning Transmission Electron Microscopy working in High Angle Annular Dark-Field mode (STEM-HAADF), High Resolution Transmision Electron Microscopy (HRTEM), Energy-dispersive X-ray Spectroscopy (X-EDS), Electron Energy Loss Spectroscopy (EELS) and Energy Filtered Transmision Electron Microscopy (EFTEM) have been used to characterise the morphology, structure and chemical composition of the nanotubes. The results indicate that nanotubes are formed by nanocrystals of cerium and praseodymium mixed oxide. Furthermore, the system $Ce_{0.8}Pr_{0.2}O_{2-\delta}$–NT/AAO shows a better performance in the CO oxidation reaction than both powdered $Ce_{0.8}Pr_{0.2}O_{2-\delta}$ prepared by conventional methods and CeO_2–NT/AAO. These results have been discussed and related to the synergistic effect of doping and nanostructuration of CeO_2.

1. Introduction

The presence of electrons in the 4f subshell lends the lanthanide elements remarkable electronic, structural, and magnetic properties which have attracted much interest both in fundamental research and in applied sciences [1]. CeO_2 is one of the lanthanide-containing compound most widely studied showing a number of applications such as catalysts [2–5], solid electrolites in fuel cells [6,7], abrasives [8], component of optic films [9] or sensors [10,11]. Among these applications, catalysis is one of the most important ones for CeO_2, which relies on the capability of this oxide to exchange oxygen with its surroundings by creating/removing oxygen vacancies in its fluorite structure. The ability to uptake/release oxygen, is usually quantified through measurements of the so called Oxygen Storage Capacity (OSC). Due to its redox behaviour, ceria has been successfully employed as a catalyst or a catalyst support for a variety of reactions which involve the exchange of oxygen between the reactants, as it is the case of those related to Three-Way Catalysis in exhaust-gas converters of gasoline-fueled vehicles [12–14] and, more recently, to those related to the production of H_2 for fuel cells [15–17] or to the abatement of organic pollutants from industrial wastewater [18,19].

The redox behaviour of ceria can be improved by means of two approaches. On one hand, transition metals (specially Zr) or lanthanide elements (Pr, Tb,) have been traditionally added to CeO_2 as alio cations in order to improve the low temperature redox response and the thermal stability. On the other hand, the precise control of the nanostructure has proven to be an effective method to modify the properties of a wide range of materials, including complex catalytic systems. For this reason several synthesis methods that yield nanostructured CeO_2 (nanotubes, nanorods, nanowires, nanopolyhedra, etc.) have been developed. These nanostructured CeO_2 oxides demonstrate enhanced catalytic behavior compared with bulk CeO_2 obtained by conventional synthesis methods [20–22]. However, only a few papers focus on the use of both mixing with a second metallic element and nanostructuration to improve the performance of CeO_2-based materials [23,24]. Among them, Pr-doped CeO_2 nanostructures are those to which more attention has been paid [25,26]. Thus, Yan et al. [25] prepared Pr-doped ceria nanorods with diameters of ~30 nm and with a length of ~400 nm via a high-temperature precipitation and subsequent low-temperature aging route. Similarly, Ren et al. [26] recently synthesized Pr-doped ceria nanorods with diameter and length ranging from 10 to 18 nm and 200 to 400 nm, respectively. It is well known that the incorporation of Pr to ceria structure

* Corresponding author. Tel.: +34 956016154; fax: +34 956016154.
E-mail address: Javier.botana@uca.es (F.J. Botana).

0920-5861/$ – see front matter © 2011 Elsevier B.V. All rights reserved.
doi:10.1016/j.cattod.2011.05.006

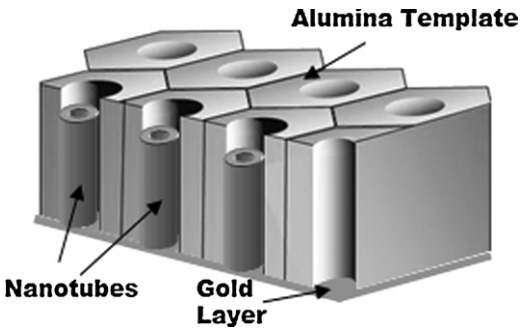

Fig. 1. Cross section scheme of the system obtained after the electrodeposition within the anodic alumina membrane.

modifies the redox properties and thermal stability of pure ceria and its catalytic behavior as well [27–29]. However, no study on the catalytic activity of Pr-doped 1D ceria nanostructures has been reported yet.

In the present work, Pr-doped CeO_2 nanotubes have been synthesized for the first time and characterized with various techniques. FEG-SEM, STEM-HAADF, HREM, X-EDS, EELS and EFTEM techniques were employed to study the morphology, structure, and chemical composition of these nanotubes. Moreover, the catalytic activity in the CO oxidation reaction of the samples prepared has been evaluated.

2. Experimental

2.1. Sample preparation

A template-based electrodeposition method was employed to synthesize the nanotubes following a procedure similar to that previously reported in [22,30]. Whatman Anodisc commercial anodic alumina membranes with a thickness of 60 μm and with pore diameters of approximately 200 nm, were employed as a template. In order to allow the membrane to be utilized as the cathode of a three-electrode electrochemical cell a thin layer of gold was deposited on one of the faces of these membranes to assure electric contact during the synthesis. SEM images confirmed that the layer of gold deposited did not block the pores of the face covered with gold. A net of platinum wires was used as the auxiliary electrode, and a Ag/AgCl 3 M electrode as reference electrode. The electrodeposition was performed for a period of 1 h in a mixed solution of 0.04 M in $Ce(NO_3)_3$ and 0.01 M in $Pr(NO_3)_3$ at ambient temperature in the galvanostatic regime, applying 1 mA cm^{-2}. The solution was added to the cell 1 h before starting the electrodeposition to assure that the pores were completely filled. Since the chemistry of praseodymium compounds is very similar to that of their equivalent of cerium, we can expect that the nanostructures formed using the proposed synthesis route, which in fact promotes the co-precipitation of the cations via electro-reduction of their nitrates, will be made up of $Ce(OH)_3$ and $Pr(OH)_3$ as already reported in [22,31,32]. Finally, the nanotube/membrane systems were oxidized at 250 °C in air for 1 h.

Fig. 1 shows a cross section scheme of the nanotube/template system obtained. After the synthesis the nanotubes were separated from the template to study their morphology, structure and composition. For this purpose, the gold film was first dissolved by immersing the nanotube/template assemblies in a 6 mM I_2 and 6 mM KI ethanolic solution for 30 min at room temperature. Secondly, the alumina template was dissolved by immersion in a aqueous solution of 1 M NaOH at 45 °C for 3 h. Finally, the resulting solid product was thoroughly rinsed with ethanol.

2.2. Characterization of the nanotubes

The as-prepared nanomaterials were characterized by means of XRD using a Bruker D8 ADVANCE diffractometer (CuKα radiation). FEG-SEM images of the nanotubes and X-EDS spectra were acquired in a FEI SIRION microscope equipped with a EDAX Phoenix system. STEM-HAADF images, HREM images and DDPs were obtained in a JEOL2010F microscope equipped with an HAADF detector, working at 200 kV. Moreover, EELS and EFTEM analysis was performed with an spectrometer (GIF2000 Gatan Imaging Filter) installed in the JEOL2010F microscope. All EEL spectra were recorded in STEM mode using a energy dispersion of 0.3 eV/channel and acquisition times of 0.3–1.0 s. Energy filtered images were recorded with an energy selecting slit of 5 eV and the acquisition time was 5 s. Elemental distribution images of Ce and Pr were obtained using the three window technique [33].

The morphological information was obtained analysing FEG-SEM and STEM-HAADF images. A structural characterisation was accomplished using XRD patterns, HREM images and their corresponding DDPs. Finally, X-EDS and EELS spectra were studied to elucidate the chemical composition of the samples.

2.3. Catalytic measurements

The catalytic activity of the nanotubes/membrane system, namely $Ce_{0.8}Pr_{0.2}O_{2-\delta}$–NT/AAO, was evaluated in the CO oxidation reaction. For comparison, the activity of an AAO gold sputtered template sample and that of a $Ce_{0.8}Pr_{0.2}O_{2-\delta}$ powdered sample from Grace were also measured. Furthermore, previously reported results for a CeO_2–NT/AAO [22] sample were also taken into account within the discussion. The experiments were carried out in a quartz reactor with 55.0 mg total amount of sample. In the essay of $Ce_{0.8}Pr_{0.2}O_{2-\delta}$–NT/AAO the amount of sample contained 10 mg of ceria–praseodymia nanotubes. Prior to the study of the catalytic activity, each sample was pretreated as follows: (1) heating from ambient temperature up to 250 °C (10 °C min^{-1}) under a flow (60 cm^3 min^{-1}) of O_2(5%)/He; (2) keeping at 250 °C for 1 h; (3) cooling down to 125 °C; (4) changing the atmosphere to pure He, and (5) cooling to ambient temperature. A reaction mixture of 1% CO + 20% O_2 balanced with He and a total flow of 60 cm^3 min^{-1} was employed for CO oxidation catalytic tests. Light-off curves were performed from room temperature up to 700 °C at a heating rate of 10 °C min^{-1}. The gases at the outlet of the reactor were analyzed with a Pfeiffer Prisma mass spectrometer.

3. Results and discussion

3.1. Morphology

Fig. 2 depicts two representative FEG-SEM images of the material prepared inside the pores of the alumina membrane. In the low magnification image, Fig. 2(a), 1D nanostructure arrays densely packed and attached to a base layer can be seen. This kind of images has been previously observed in CeO_2 nanotubes prepared using a similar procedure [22,30]. High magnification image, Fig. 2(b), reveals the presence of hollow structures, thus indicating that they are nanotubes. These images also suggest irregularities at the nanotube walls as cracks and holes of different size. The diameter of the nanotubes which can be estimated from these images is close to 300 nm, i.e. larger than the template pore size, 200 nm. The reasonable explanation to account for this observation is that the cerium praseodymium mixed oxide nanostructure collapses after being extracted from the template. Very likely, the nanotube walls are not rigid enough to keep their shape after removing the alumina template.

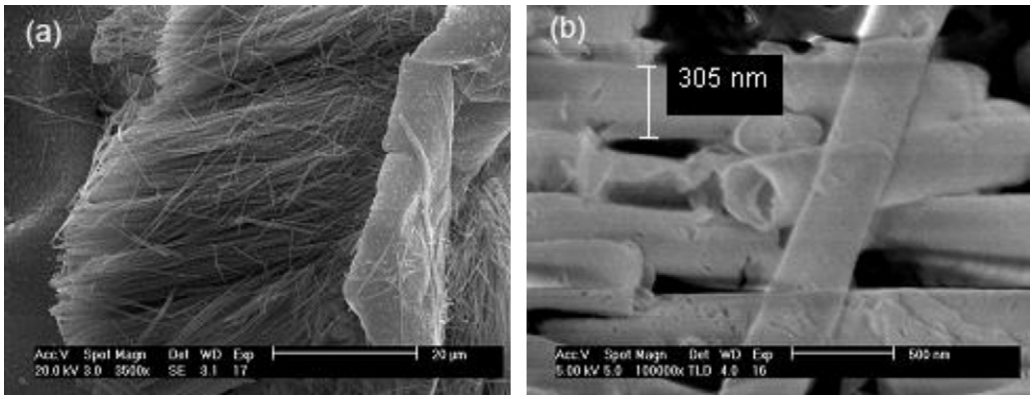

Fig. 2. FEG-SEM images of $Ce_{0.8}Pr_{0.2}O_{2-\delta}$ nanotubes.

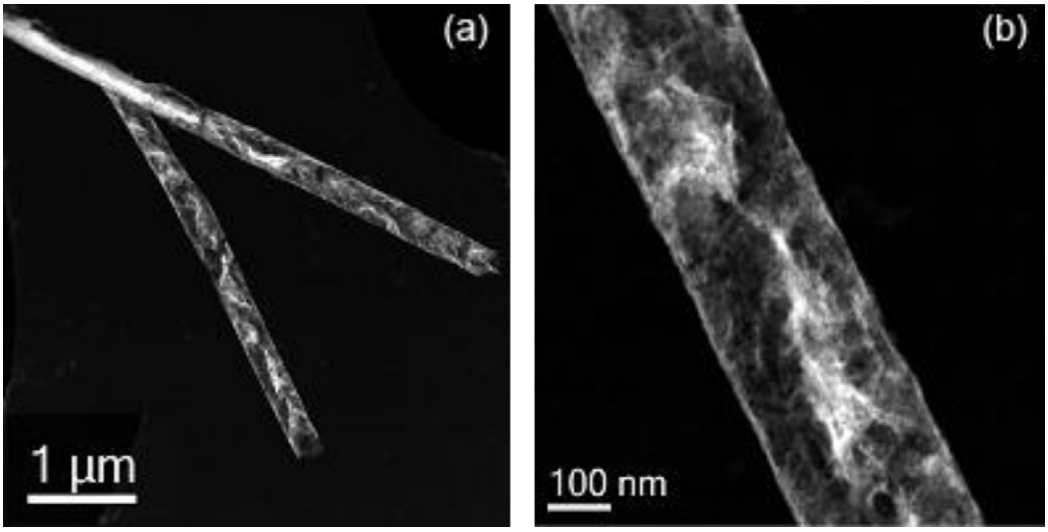

Fig. 3. STEM-HAADF images of $Ce_{0.8}Pr_{0.2}O_{2-\delta}$ nanotubes.

Fig. 3 shows two STEM-HAADF images of the nanotubes. The bright bands expected for tubular shapes can be observed at the edges of the nanostructures. Note however that the images show also bright contrasts in areas inside the tube walls. This could be due either to folding towards the inner side of the tube of torn portions of the tube walls or to the development of an inner wall system, as previously reported for ceria nanotubes [22].

3.2. Structure

In Fig. 4(a) XRD pattern of the cerium praseodymium mixed oxide nanotubes extracted from the template is included. The peaks at 28.50°, 33.05°, 47.45° and 56.20° in this diffractogram can be indexed to a fluorite-like structure with cell parameter of $a = 5.420$ Å, very close to that of CeO_2, $a = 5.411$ (ICDD card 034-0394). No other phase could be detected in the XRD pattern of this sample. According to the literature [25,28,29,34], $Ce_xPr_{1-x}O_{2-\delta}$ solid solutions can be formed in the range $x = 1$–0.7. In this situation, Pr fully incorporates into the cubic structure of CeO_2, replacing Ce in the cationic octahedral positions. This substitution is facilitated by two factors: (a) the structural similarity of CeO_2 and Pr_6O_{11}, both cubic fluorite-type; and (b) the similarity between the ionic radius of Ce(IV), 0.97 Å, and Pr(IV), 0.96 Å. This seems to be the case of the as-prepared nanotubes. Another feature of the XRD pattern in Fig. 4 is that the peaks are very broad, surely due to the existence of very tiny crystallites.

In order to characterize further the structure of the nanotubes, HREM images were acquired and corresponding digital diffraction patterns (DDPs) were generated calculating the fast Fourier transform of the images or parts of them. HREM images in Fig. 5 show

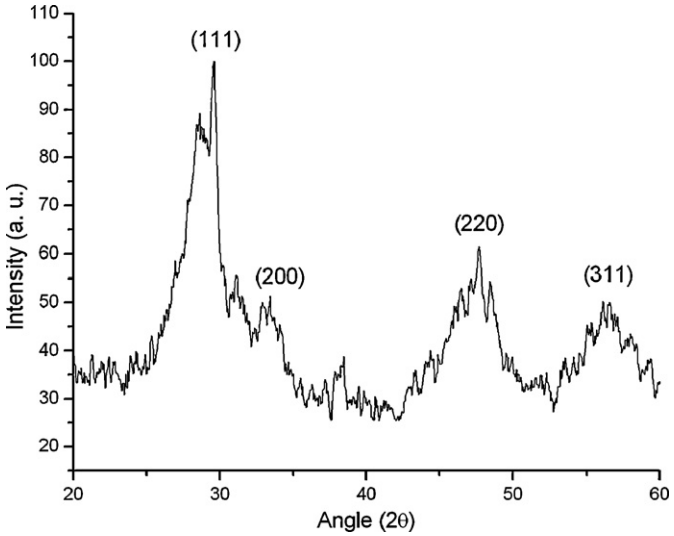

Fig. 4. XRD pattern of $Ce_{0.8}Pr_{0.2}O_{2-\delta}$ nanotubes.

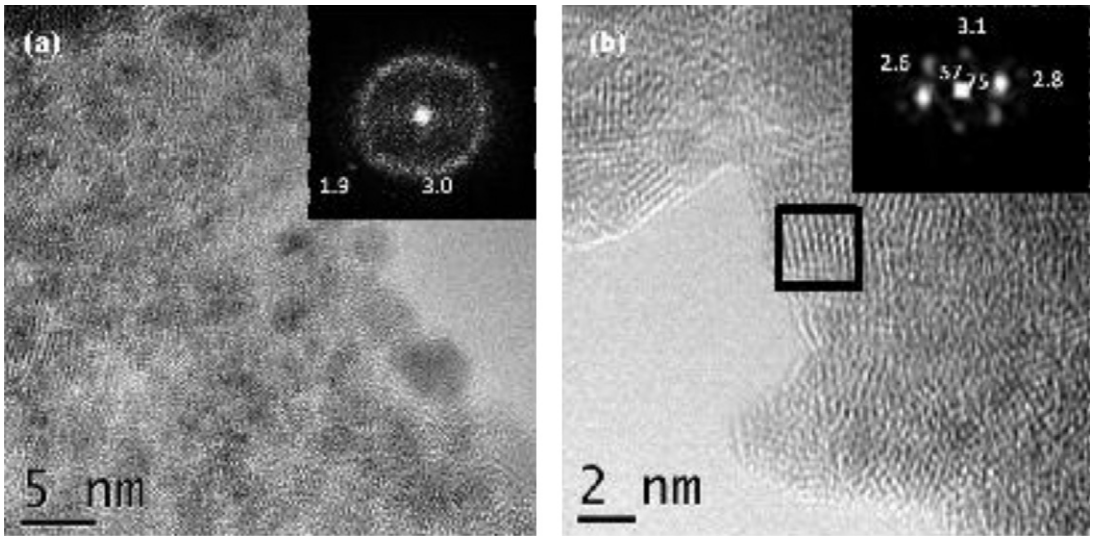

Fig. 5. HREM images and corresponding DDPs of a $Ce_{0.8}Pr_{0.2}O_{2-\delta}$ nanotube.

1–5 nm sized nanocrystals randomly oriented to each other and densely packed. The DDP of this image, Fig. 5(a), shows a ring of diffraction spots corresponding to a lattice spacing of 3.0 Å, very close to that of the (1 1 1) planes of CeO_2, 3.12 Å. DDPs from smaller areas, like that in Fig. 5(b) which was calculated from the area marked with a square, can also be assigned to a fluorite-type phase with a lattice parameter slightly shorter than that of pure CeO_2. In particular, the DDP in this figure corresponds to fluorite in [1 1 0] direction.

The HREM results just described agree with XRD patterns, this indicating that Pr fully incorporates to the CeO_2 matrix to form a cerium praseodymium mixed oxide which maintains the cubic fluorite structure.

3.3. Chemical composition

Fig. 6 shows an X-EDS spectrum acquired on the $Ce_{0.8}Pr_{0.2}O_{2-\delta}$ nanotubes. The main signals correspond to Ce, Pr and O. Au, Ag and Al peaks are also present in this sample. Aluminum signals arise from undissolved alumina template remains. The gold peaks are due to the gold film which is sputter over the sample to avoid charge phenomena during SEM analysis. Silver was used to fix the sample on the SEM stage. The semiquantitative analysis of X-EDS

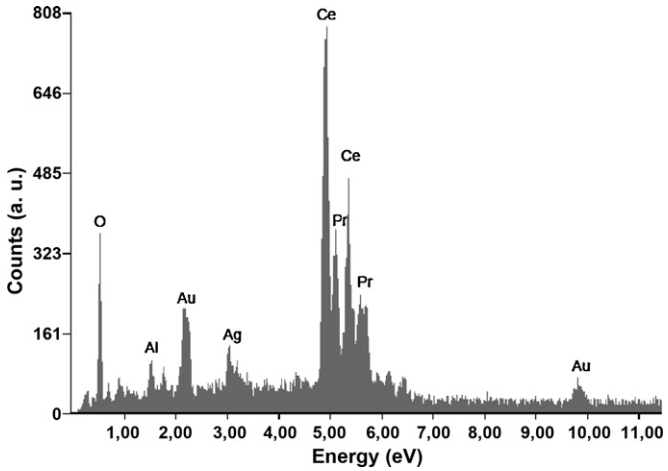

Fig. 6. X-EDS spectrum of $Ce_{0.8}Pr_{0.2}O_{2-\delta}$ nanotubes after being extracted from the template.

leads to a Ce/Pr molar ratio of $75/25 \pm 1.5$, a value slightly different to that of the nominal starting solution (80/20).

Further quantitative X-EDS-STEM analysis carried out in spot mode with a subnanometer electron probe allowed us stablising the following molar contents: $75 \pm 3.5\%$ for Ce and $25 \pm 3.5\%$ for Pr, in good agreement with SEM X-EDS semiquantitative analysis.

To gain more detailed information about the chemical composition of the nanotubes, an STEM-EELS study was carried out using a 0.5 nm diameter electron probe. The STEM-HAADF image of Fig. 7(a) depicts a nanotube on which a series of 64 EELS spectra were acquired along the line marked on Fig. 7, at steps of 0.5 nm. The spectra included in Fig. 7(b) are showed separately as an example. According to the literature [35,36], Ce gives rise to the two peaks at 900–950 eV, whilst the two peaks located around 1000–1050 eV come from Pr.

These EEL spectra have also allowed us estabilishing in qualitative terms the oxidation state of Ce and Pr [36,37] in the nanotubes. Thus, the small shoulders on the right side of Ce signals clearly indicate that the sample contains Ce(IV). However, the relative intensities of the M_4 and M_5 signals indicates that also a fraction of Ce(III) is present. In the case of the Pr signals, the intensity of the M_5 line is nearly two-fold that of M_4, a feature which indicates that this element is mainly present in the nanotube as Pr(III). The absence of the shoulder at the lower energy side of the M_4 confirms further this idea. Thus, from a redox point of view EELS suggest that in the solid solution the lanthanide elements are present as a mixture of Ce(III)/Ce(IV), in the case of cerium, and mainly as Pr(III) in the case of praseodymium. This finding is consistent with the literature, since both elements have proven to have +3 and +4 oxidation states that are readily formed in ceria–praseodymia solid solutions [38,39].

Fig. 7(c) displays an EFTEM image of a zone of a nanotube. In this image, Ce $M_{4,5}$ signals have been coloured in red and Pr $M_{4,5}$ signals in yellow. Note the coexistence of Ce and Pr in the analyzed area, which it becomes evident by the general green appearance of the image. Therefore, this result proves that the ceria–praseodimia solid solution is highly homogeneous regarding chemical composition.

3.4. Catalytic activity

The results of the CO oxidation essays carried out on the synthesized nanotubes and the corresponding reference materials are

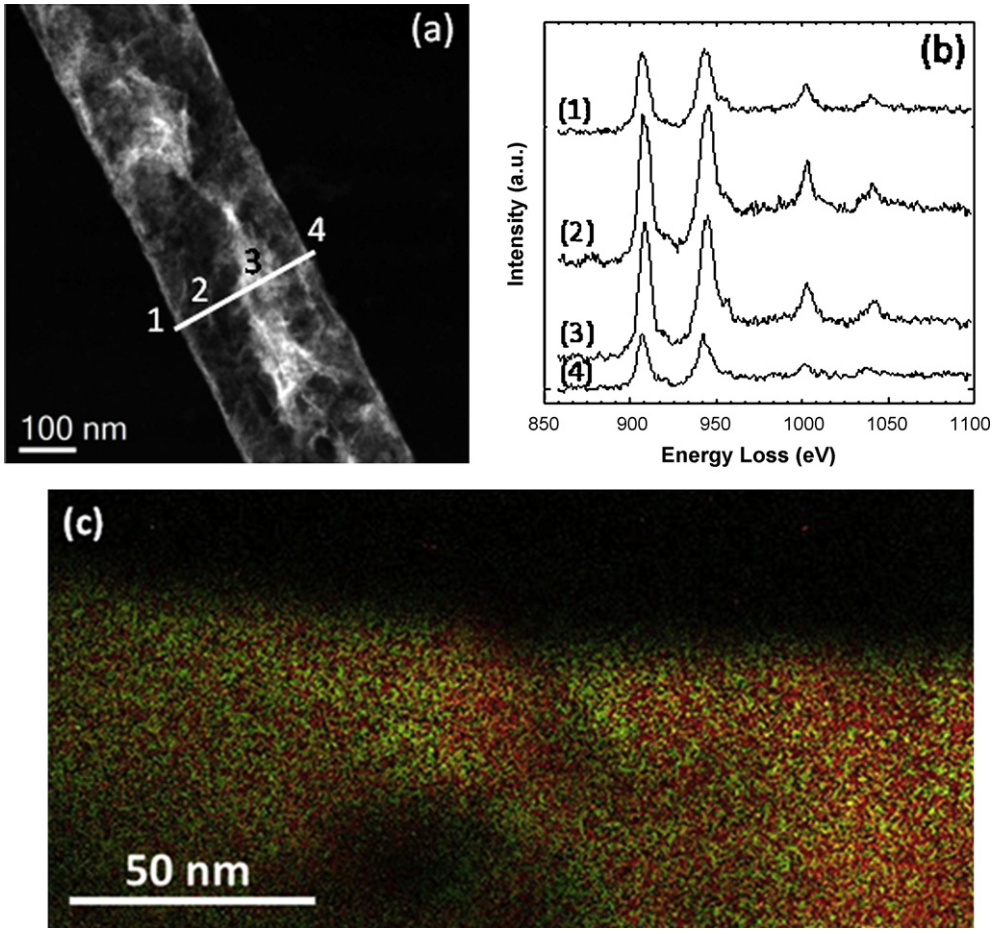

Fig. 7. (a) STEM-HAADF image showing the section of a $Ce_{0.8}Pr_{0.2}O_{2-\delta}$ nanotube analyzed by EELS; (b) selected EELS spectra acquired along the line marked in image (a); (c) elemental maps of Ce $M_{4,5}$ (red) and Pr $M_{4,5}$ (yellow) obtained by EFTEM. (For interpretation of the references to color in this figure legend, the reader is referred to the web version of the article.)

plotted in Fig. 8, which includes the light-off traces of the following systems: (1) Ce–Pr nanotubes/membrane: $Ce_{0.8}Pr_{0.2}O_{2-\delta}$–NT/AAO; (2) CeO_2 nanotubes/membrane: CeO_2–NT/AAO; (3) a Ce–Pr mixed oxide powder sample: $Ce_{0.8}Pr_{0.2}O_{2-\delta}$ and (4) gold sputtered membrane: Au/AAO.

According to Fig. 8, the light-off temperature over the $Ce_{0.8}Pr_{0.2}O_{2-\delta}$ powder is 360 °C, whereas over the newly prepared $Ce_{0.8}Pr_{0.2}O_{2-\delta}$–NT/AAO system is only 157 °C. Regarding the CeO_2–NT/AAO system, the previously reported T_{50} was 189 °C [22]. These results indicate therefore that the system containing the ceria–praseodymia nanotubes ($Ce_{0.8}Pr_{0.2}O_{2-\delta}$–NT/AAO) performs better than both the powdered ($Ce_{0.8}Pr_{0.2}O_{2-\delta}$) oxide and the system containing the ceria nanotubes (CeO_2–NT/AAO). Large differences do exist between the reaction rates of the different samples in the low temperature range. Thus, at 200 °C, the rates of CO conversion over the $Ce_{0.8}Pr_{0.2}O_{2-\delta}$–NT/AAO, $Ce_{0.8}Pr_{0.2}O_{2-\delta}$ and CeO_2–NT/AAO catalysts are 1.16, 0.001 and 0.77 cm^3 CO (STP)/g s (per gram of oxide), respectively. Therefore, the reaction rate over $Ce_{0.8}Pr_{0.2}O_{2-\delta}$–NT/AAO is roughly 1000 and 1.5 times higher than that over $Ce_{0.8}Pr_{0.2}O_{2-\delta}$ powder and CeO_2–NT/AAO, respectively.

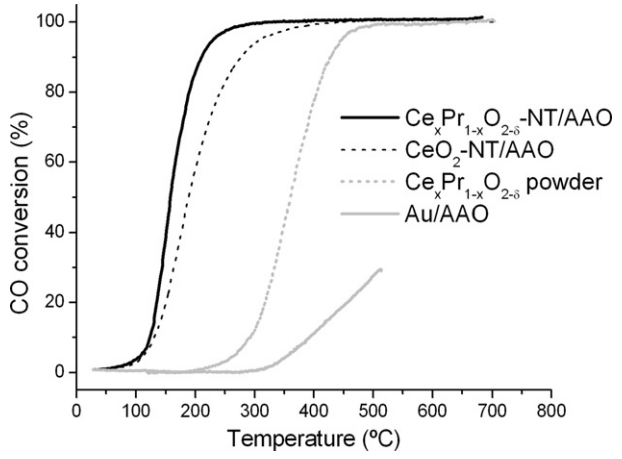

Fig. 8. CO conversion *vs* temperature reaction curves of $Ce_{0.8}Pr_{0.2}O_{2-\delta}$–NT/AAO, $Ce_{0.8}Pr_{0.2}O_{2-\delta}$ powder, CeO_2–NT/AAO and Au/AAO.

As shown in Fig. 8, the alumina template coated with gold is much less active than any of the other systems. The activity of Au/AAO is negligible below 300 °C, a temperature at which $Ce_{0.8}Pr_{0.2}O_{2-\delta}$–NT/AAO and CeO_2–NT/AAO allow almost 100% CO conversion. This indicates that the gold layer deposited as electrode at the bottom of the alumina membrane does not play by itself an important role in the CO oxidation reaction.

Regarding with the effects of Pr-doping on the catalytic activity of the nanotubes, the characterization work presented in this paper clearly proves that Pr incorporates into the fluorite ceria matrix in the form of a solid solution which present an homogeneous composition along the tube structure. The co-existence of Ce(III)/Ce(IV) and Pr(III) ions in the nanotubes, predicted by the literature and confirmed by our EELS studies, gives rise to a higher concentration

of oxygen vacancies related to Pr(III) which can eventually lead to an improved oxygen mobility in the mixed oxide with respect to that of the pure ceria nanotubes [27–29,38,40]. This improvement in oxygen handling could justify the better catalytic performance in the CO oxidation reaction of the $Ce_{0.8}Pr_{0.2}O_{2-\delta}$–NT/AAO system as compared to the CeO_2–NT/AAO system.

The differences between the nanostructured materials, those in the form of nanotubes, and those in the form of powders require a more in depth analysis. Although this issue is still challenging, a detailed review of the literature suggests that some features of the peculiar nanostructuration reached by the template-assisted electrodeposition method used in this work could have a significant contribution to the improvement in catalytic performance. Firstly, nanosized crystallites may exhibit quantum-size effects. In fact, it has been found recently that small clusters of $Ce_mO_{2m}^+$ (m = 2–6) are more reactive than larger ones in CO and small organic molecules oxidation reactions [41], the active site in these reactions being a OCeO moiety. The authors propose that radical type centers similar to those identified in $Ce_mO_{2m}^+$ (m = 2-6) may exist over bulk CeO_2 or related materials through charge transfer, photon excitation, or mixing/doping other oxides with CeO_2. Secondly, the densely packed and randomly oriented crystalittes may expose at their surface more reactive planes and regions of lower oxygen coordinations such as edges, vertexes or grain boundaries [20,21,42], which may provide a higher density of active sites for heterogenous reactions. Thirdly, at upper level, the tubular shape allows both a high surface area and easy diffusion of the gases in the reaction mixture. In any case, to ascertain the impact of these quite peculiar nanostructural features on CO oxidation catalytic activity, a more in depth research is required. In this additional research work should be assessed, among others, the role of other relevant structural features as it is the presence of the Au/nanotube interface in the $Ce_{0.8}Pr_{0.2}O_{2-\delta}$–NT/AAO system. Work is under progress in our lab to improve our current understanding of the exact role of the nanostructuration effects induced by the synthetic approach we have used in this paper.

Given that the nanostructural features of pure ceria and ceria–praseodimia nanotubes are fairly the same, our data prove that the addition of praseodimium during the electrodeposition process results in materials with significantly improved catalytic performance.

4. Conclusions

Cerium-praseodymium mixed oxide nanotubes have been prepared and characterized for the first time. A convenient and fast synthesis method based on electrodeposition inside the pores of anodic alumina oxide templates has been employed. The samples obtained have been characterized morphologically, chemically and structurally by means of various electron microscopy techniques. The main results of this characterization work show that the samples are nanotubes formed by cerium–praseodymium mixed oxide nanocrystals (1–5 nm) with a cubic fluorite-type structure whose cell parameter is slightly shorter than that of pure CeO_2. Micro and nano-analysis of the tubes indicate an homogeneous distribution of the two lanthanide elements along the tubes with a Ce/Pr molar ratio close to 72/25. Moreover, the co-existence of Ce(III)/Ce(IV) and Pr(III)/Pr(IV) in the prepared nanomaterials has been proved.

The catalytic activity of the samples prepared and those of other reference materials were evaluated and discussed. Although there are ongoing studies to understand in more details the catalytic performance of the oxide-NT/AAO systems, some conclusions can be claimed so far. Thus, the CO oxidation reaction at 200 °C over the newly prepared $Ce_{0.8}Pr_{0.2}O_{2-\delta}$–NT/AAO system has proven to be roughly 1000 times faster than over powder $Ce_{0.8}Pr_{0.2}O_{2-\delta}$ obtained with conventional methods and 1.5 times higher than over CeO_2–NT/AAO. The differences have been tentatively attributed to the improvement of the redox properties induced by the incorporation of Pr into the CeO_2 lattice and the likely influence of the nanostructure. Thus, both doping and nanostructuration can be simultaneously exploited to enhance the catalytic performance of ceria-based materials.

Acknowledgements

This work has received financial support from MICINN-FEDER (Proj. Ref. CSD2009-00013 and MAT2008-00889-NAN). J.J. Delgado and X. Chen thank the Junta de Andalucía (Proj. Ref. FQM-3994). X. Chen acknowledges the Ramón y Cajal program from Spanish Ministry of Science and Innovation. Electron microscopy data were obtained at DME-SCCyT UCA.

References

[1] H.C. Aspinall, Chemistry of the f-block Elements, Amsterdam, 2001.
[2] A. Trovarelli, Catalysis by Ceria and Related Materials , Imperial Collegue Press, London, 2002.
[3] M.G.J. Kašpar, P. Fornasiero, Handbook on the Physics and Chemistry of Rare Earth: The Role of Rare Earth in Catalysis , Springer, Berlín, 2000.
[4] C.T. Campbell, C.H.F. Peden, Oxygen vacancies and catalysis on ceria surfaces , Science 309 (2005) 713–714.
[5] J. Kašpar, P. Fornasiero, M. Graziani, Use of CeO_2-based oxides in the three-way catalysis , Catalysis Today 50 (1999) 285–298.
[6] C. Xia, M. Liu, Low-temperature SOFCs based on $Gd_{0.1}Ce_{0.9}O_{1.95}$ fabricated by dry pressing , Solid State Ionics 144 (2001) 249–255.
[7] H.T. Chen, J.G. Chang, H.L. Chen, S.P. Ju, Identifying the O_2 diffusion and reduction mechanisms on CeO_2 electrolyte in solid oxide fuel cells: a DFT + U study , Journal of Computational Chemistry 30 (2009) 2433–2442.
[8] X. Feng, D.C. Sayle, Z.L. Wang, M.S. Paras, B. Santora, A.C. Sutorik, T.X.T. Sayle, Y. Yang, Y. Ding, X. Wang, Y.S. Her, Converting ceria polyhedral nanoparticles into single-crystal nanospheres , Science 312 (2006) 1504–1508.
[9] Y.W. Zhang, R. Si, C.S. Liao, C.H. Yan, C.X. Xiao, Y. Kou, Facile alcohothermal synthesis, size-dependent ultraviolet absorption, and enhanced CO conversion activity of ceria nanocrystals , Journal of Physical Chemistry B 107 (2003) 10159–10167.
[10] N. Izu, W. Shin, N. Murayama, Fast response of resistive-type oxygen gas sensors based on nano-sized ceria powder , Sensors and Actuators, B: Chemical 93 (2003) 449–453.
[11] X.Q. Fu, C. Wang, H.C. Yu, Y.G. Wang, T.H. Wang, Fast humidity sensors based on CeO_2 nanowires , Nanotechnology 18 (2007).
[12] A. Trovarelli, Catalytic properties of ceria and CeO_2-Containing materials , Catalysis Reviews - Science and Engineering 38 (1996) 439–520.
[13] R.J. Farrauto, R.M. Heck, Catalytic converters: state of the art and perspectives , Catalysis Today 51 (1999) 351–360.
[14] J. Kaspar, P. Fornasiero, N. Hickey, Automotive catalytic converters: current status and some perspectives , Catalysis Today 77 (2003) 419–449.
[15] C.H. Kim, L.T. Thompson, On the importance of nanocrystalline gold for Au/CeO_2 water-gas shift catalysts , Journal of Catalysis 244 (2006) 248–250.
[16] S. Carrettin, P. Concepción, A. Corma, J.M. López Nieto, V.F. Puntes, Nanocrystalline CeO_2 increases the activity of Au for CO oxidation by two orders of magnitude , Angewandte Chemie - International Edition 43 (2004) 2538–2540.
[17] Q. Fu, W. Deng, H. Saltsburg, M. Flytzani-Stephanopoulos, Activity and stability of low-content gold–cerium oxide catalysts for the water–gas shift reaction , Applied Catalysis B: Environmental 56 (2005) 57–68.
[18] D. Goi, C. De Leitenburg, A. Trovarelli, G. Dolcetti, Catalytic wet-oxidation of a mixed liquid waste: COD and AOX abatement , Environmental Technology 25 (2004) 1397–1403.
[19] G. Blanco, M.A. Cauqui, J.J. Delgado, A. Galtayries, J.A. Pérez-Omil, J.M. Rodríguez-Izquierdo, Preparation and characterization of Ce–Mn–O composites with applications in catalytic wet oxidation processes , Surface and Interface Analysis 36 (2004) 752–755.
[20] H.X. Mai, L.D. Sun, Y.W. Zhang, R. Si, W. Feng, H.P. Zhang, H.C. Liu, C.H. Yan, Shape-selective synthesis and oxygen storage behavior of ceria nanopolyhedra, nanorods, and nanocubes , Journal of Physical Chemistry B 109 (2005) 24380–2439024385.
[21] K. Zhou, X. Wang, X. Sun, Q. Peng, Y. Li, Enhanced catalytic activity of ceria nanorods from well-defined reactive crystal planes , Journal of Catalysis 229 (2005) 206–212.
[22] L. González-Rovira, J.M. Sánchez-Amaya, M. López-Haro, E. Del Rio, A.B. Hungría, P. Midgley, J.J. Calvino, S. Bernal, F.J. Botana, Single-step process to prepare CeO_2 nanotubes with improved catalytic activity , Nano Letters 9 (2009) 1395–1400.
[23] Y. Xin, Y. Qi, X. Ma, Z. Wang, Z. Zhang, S. Zhang, Rare-earth (Nd, Sm, Eu, Gd and Y) enhanced CeO_2 solid solution nanorods prepared by co-precipitation without surfactants , Materials Letters 64 (2010) 2659–2662.

[24] Y.C. Chen, K.B. Chen, C.S. Lee, M.C. Lin, Direct synthesis of Zr-doped ceria nanotubes , Journal of Physical Chemistry C 113 (2009) 5031–5034.
[25] L. Yan, X. Xing, R. Yu, L. Qiao, J. Chen, J. Deng, G. Liu, Synthesis of Pr-doped ceria nanorods with a high specific surface area , Scripta Materialia 56 (2007) 301–304.
[26] Y. Ren, C. Deng, D. Ai, J. Ma, Q. Zan, J. Kong, J. Xu, A facile template-free synthesis of praseodymium-doped ceria nanorods , Key Engineering Materials (2010) 714–716.
[27] Z.Y. Pu, J.Q. Lu, M.F. Luo, Y.L. Xie, Study of oxygen vacancies in $Ce_{0.9}Pr_{0.1}O_{2-\delta}$ solid solution by in situ X-ray diffraction and in situ Raman spectroscopy , Journal of Physical Chemistry C 111 (2007) 18695–18702.
[28] Z.Y. Pu, X.S. Liu, A.P. Jia, Y.L. Xie, J.Q. Lu, M.F. Luo, Enhanced activity for CO oxidation over Pr- and Cu-doped CeO_2 catalysts: effect of oxygen vacancies , Journal of Physical Chemistry C 112 (2008) 15045–15051.
[29] M.F. Luo, Z.L. Yan, L.Y. Jin, Structure and redox properties of $Ce_xPr_{1-x}O_{2-\delta}$ mixed oxides and their catalytic activities for CO, CH_3OH and CH_4 combustion , Journal of Molecular Catalysis A: Chemical 260 (2006) 157–162.
[30] L. González-Rovira, J.M. Sánchez-Amaya, M. López-Haro, A.B. Hungria, Z. Boukha, S. Bernal, F.J. Botana, Formation and characterization of nanotubes of $La(OH)_3$ obtained using porous alumina membranes , Nanotechnology 19 (2008).
[31] P. Bocchetta, M. Santamaria, F. Di Quarto, Electrosynthesis of Ce–Co mixed oxide nanotubes with high aspect ratio and tunable composition , Electrochemical and Solid-State Letters 11 (2008) K27–K30.
[32] P. Bocchetta, M. Santamaria, F. Di Quarto, From ceria nanotubes to nanowires through electrogeneration of base , Journal of Applied Electrochemistry 39 (2009) 2073–2081.
[33] R.F. Egerton, Electron Energy-Loss Spectroscopy in the Electron Microscope , Plenum Press, New York, 1986.
[34] S. Bernal, G. Blanco, M.A. Cauqui, A. Martín, J.M. Pintado, A. Galtayries, R. Sporken, Oxygen buffering capacity (OBC) of praseodymium-modified CeO_2: influence of the Pr distribution in the ceria host lattice , Surface and Interface Analysis 30 (2000) 85–89.
[35] T. Manoubi, C. Colliex, P. Rez, Quantitative electron energy loss spectroscopy on M45 edges in rare earth oxides , Journal of Electron Spectroscopy and Related Phenomena 50 (1990) 1–18.
[36] C. López-Cartes, S. Bernal, J.J. Calvino, M.A. Cauqui, G. Blanco, J.A. Pérez-Omil, J.M. Pintado, S. Helveg, P.L. Hansen, In situ transmission electron microscopy investigation of Ce(IV) and Pr(IV) reducibility in a Rh (1%)/$Ce_{0.8}Pr_{0.2}O_{2-x}$ catalyst , Chemical Communications 9 (2003) 644–645.
[37] M.P. Rodríguez-Luque, J.C. Hernández, M.P. Yeste, S. Bernal, M.A. Cauqui, J.M. Pintado, J.A. Pérez-Omil, O. Stéphan, J.J. Calvino, S. Trasobares, Preparation of rhodium/$Ce_xPr_{1-x}O_2$ catalysts: a nanostructural and nanoanalytical investigation of surface modifications by transmission and scanning-transmission electron microscopy , Journal of Physical Chemistry C 112 (2008) 5900–5910.
[38] Z. Song, W. Liu, H. Nishiguchi, A. Takami, K. Nagaoka, Y. Takita, The Pr promotion effect on oxygen storage capacity of Ce–Pr oxides studied using a TAP reactor , Applied Catalysis A: General 329 (2007) 86–92.
[39] B.M. Reddy, G. Thrimurthulu, L. Katta, Y. Yamada, S.E. Park, Structural characteristics and catalytic activity of nanocrystalline ceria–praseodymia solid solutions , Journal of Physical Chemistry C 113 (2009) 15882–15890.
[40] Z.C. Kang, L. Eyring, Lattice oxygen transfer in fluorite-type oxides containing Ce, Pr, and/or Tb , Journal of Solid State Chemistry 155 (2000) 129–137.
[41] X.N. Wu, Y.X. Zhao, W. Xue, Z.C. Wang, S.G. He, X.L. Ding, Active sites of stoichiometric cerium oxide cations ($Ce_mO_{2m}^+$) probed by reactions with carbon monoxide and small hydrocarbon molecules , Physical Chemistry Chemical Physics 12 (2010) 3984–3997.
[42] C. Pan, D. Zhang, L. Shi, CTAB assisted hydrothermal synthesis, controlled conversion and CO oxidation properties of CeO_2 nanoplates, nanotubes, and nanorods , Journal of Solid State Chemistry 181 (2008) 1298–1306.